GENETIC TESTING AND MOLECULAR BIOMARKERS
Volume 18, Number 11, 2014

Pp. 722–735
DOI: 10.1089/gtmb.2014.0109

The Use of Next-Generation Sequencing in Molecular Diagnosis of Neurofibromatosis Type 1: A Validation Study

Ryo Maruoka,[1,2] Toshiki Takenouchi,[1,3] Chiharu Torii,[1] Atsushi Shimizu,[4] Kumiko Misu,[1] Koichiro Higasa,[5] Fumihiko Matsuda,[5] Arihito Ota,[6] Katsumi Tanito,[6] Akira Kuramochi,[7] Yoshimi Arima,[8] Fujio Otsuka,[9] Yuichi Yoshida,[10] Keiji Moriyama,[2] Michihito Niimura,[6] Hideyuki Saya,[8] and Kenjiro Kosaki[1]

Aims: We assessed the validity of a next-generation sequencing protocol using in-solution hybridization-based enrichment to identify *NF1* mutations for the diagnosis of 86 patients with a prototypic genetic syndrome, neurofibromatosis type 1. In addition, other causative genes for classic genetic syndromes were set as the target genes for coverage analysis. *Results:* The protocol identified 30 nonsense, 19 frameshift, and 8 splice-site mutations, together with 10 nucleotide substitutions that were previously reported to be pathogenic. In the remaining 19 samples, 10 had single-exon or multiple-exon deletions detected by a multiplex ligation-dependent probe amplification method and 3 had missense mutations that were not observed in the normal Japanese SNP database and were predicted to be pathogenic. Coverage analysis of the genes other than the *NF1* gene included on the same diagnostic panel indicated that the mean coverage was 115-fold, a sufficient depth for mutation detection. *Conclusions:* The overall mutation detection rate using the currently reported method in 86 patients who met the clinical diagnostic criteria was 92.1% (70/76) when 10 patients with large deletions were excluded. The results validate the clinical utility of this next-generation sequencing-based method for the diagnosis of neurofibromatosis type 1. Comparable detection rates can be expected for other genetic syndromes, based on the results of the coverage analysis.

Introduction

GENETIC TESTING HAS HELPED clinicians to define the molecular pathology of diseases, especially when patients present with an atypical combination of phenotypic features. Our group developed a custom-designed mutation analysis panel using denaturing high-pressure liquid chromatography for the systematic screening of patients with classic genetic syndromes (Kosaki *et al.*, 2005). The system can be used to screen all the exons of the candidate gene quickly and has been helpful in confirming the clinical diagnosis, as published in a series of reports in this journal (Udaka *et al.*, 2005, 2006, 2007; Aramaki *et al.*, 2006; Samejima *et al.*, 2007; Hattori *et al.*, 2009). Nevertheless, the throughput of the system was not high enough to screen multiple candidate genes in a single testing.

The recent advent of a target sequencing panel with the next-generation sequencing technology has enabled many genes, regardless of size, to be analyzed in a systematic and comprehensive manner, as reviewed in this journal (Yan *et al.*, 2013). The strength of such a comprehensive approach is the ability to detect atypical presentations of classic syndromes, as illustrated by our recent reports on several patients with atypical presentations of mutations in the causative

[1]Center for Medical Genetics, Keio University School of Medicine, Tokyo, Japan.
[2]Section of Maxillofacial Orthognathics, Division of Maxillofacial/Neck Reconstruction, Department of Maxillofacial Reconstruction and Function, Graduate School, Tokyo Medical and Dental University, Tokyo, Japan.
[3]Department of Pediatrics, Keio University School of Medicine, Tokyo, Japan.
[4]Division of Biomedical Information Analysis, Iwate Tohoku Medical Megabank Organization, Iwate Medical University, Iwate, Japan.
[5]Center for Genomic Medicine, Kyoto University Graduate School of Medicine, Kyoto, Japan.
[6]Department of Dermatology, Jikei University School of Medicine, Tokyo, Japan.
[7]Department of Dermatology, Saitama Medical University, Saitama, Japan.
[8]Division of Gene Regulation, Institute for Advanced Medical Research, Keio University School of Medicine, Tokyo, Japan.
[9]Department of Dermatology, Institute of Clinical Medicine, University of Tsukuba, Tsukuba, Japan.
[10]Division of Dermatology, Department of Medicine of Sensory and Motor Organs, Faculty of Medicine, Tottori University, Yonago, Japan.

genes of three classic genetic syndromes: the neonatal progeroid presentation of an *FBN1* mutation (Takenouchi *et al.*, 2013a), the Noonan-cafe au lait syndrome-like presentation of a *MAP2K2* mutation (Takenouchi *et al.*, 2013b), and Stickler syndrome-like presentation of *SOX9* mutation (Takenouchi *et al.*, 2014).

In this study, we assessed the analytical and clinical validity of the next-generation sequencing protocol with in-solution hybridization-based enrichment to identify disease-causing mutations in the diagnosis of a prototypic genetic syndrome, neurofibromatosis type 1, compared with direct capillary sequencing, which is the current gold standard methodology. The reason for the choice of the *NF1* gene, the causative gene for neurofibromatosis type 1, was twofold: (1) neurofibromatosis type 1 is a relatively common genetic condition with readily recognizable phenotypes: café-au-lait spots, cutaneous neurofibromas, axillary and inguinal freckling, and Lisch nodules (iris hamartomas) (Carey and Viskochil, 1999) and (2) the *NF1* gene comprised a total of 58 exons and is one of the largest genes in the human genome, making it a relatively difficult clinical target for direct capillary sequencing.

Materials and Methods

Patients

The current research protocol was approved by the institutional review board of Keio University and each participating center. Eighty-six patients with neurofibromatosis type 1 who met the NIH clinical diagnostic criteria (Neurofibromatosis Conference Statement, 1988) were recruited from multiple centers participating in the project. The NIH diagnostic criteria for neurofibromatosis type 1 defines an individual as neurofibromatosis type 1 when the person has two or more of the following features: six or more café-au-lait macules with a maximum diameter of over 5 mm in prepubertal individuals and with a maximum diameter of over 15 mm in postpubertal individuals; two or more neurofibromas of any type or 1 plexiform neurofibroma; freckling in the axillary or inguinal regions; optic glioma, two or more Lisch nodules; a distinctive osseous lesion, such as sphenoid dysplasia or tibial pseudarthrosis; and a first-degree relative (parent, sibling, or offspring) with neurofibromatosis type 1, as defined according to the above-mentioned criteria. After written consent was obtained at each participating center, the whole blood samples were sent to Keio University for genetic analysis.

Genomic DNA, sample preparation, targeted capturing, sequencing

Genomic DNA was extracted from peripheral blood according to standard procedures using the phenol–chloroform extraction method and checked for quality using Qubit (Life Technologies). The genomic DNA (3 μg) was fragmented into ~150 bp. In-solution hybridization-based enrichment was performed using the SureSelect Target Enrichment system (Agilent Technologies). The *NF1* gene (the canonical Refseq transcript NM_001042492.2) together with 108 causative genes for the more common classical congenital malformation syndromes selected from a standard textbook (Jones, 2005) was set as the target gene (Table 1). Genes that are responsible for a disease phenotype and involved in the RAS pathway (i.e., Rasopathy genes) (Aoki *et al.*, 2008) were included in the 108 genes set. A biotinylated RNA capture library was designed using the eArray system (Agilent Technologies) according to the manufacturer's protocol. The captured DNA was subjected to a 150-bp paired-end read sequencing on the MiSeq system (Illumina).

Bioinformatics pipeline

The sequence reads from the sequencer were exported as FASTQ format files and were analyzed using sets of open-source programs by means of the default parameters; the sequence reads were aligned to the human reference genome DNA sequence (hs37d5 assembly) using the Burrows–Wheeler Alignment (BWA) tool version 0.6.1 (Li and Durbin, 2009). The Genome Analysis Toolkit (GATK) package (McKenna *et al.*, 2010) was used to perform local realignment, base quality score recalibration, and SNP/indel calls. The called SNPs/indels were annotated using snpEff version 3.1 (Cingolani *et al.*, 2012), regarded as nonpathogenic, and excluded from further analysis when they were observed in the 1000 Genomes Project (www.1000genomes.org/) or in the Japanese SNP dataset of 1208 normal individuals (Japanese Genetic Variation Consortium, 2013). The variants and alignments were visually inspected using the Integrative Genomics Viewer version 2.1 (Thorvaldsdóttir *et al.*, 2013) and VarSifter version 1.5 (Teer *et al.*, 2012). Variants in the RAS pathway, including *PTPN11*, *KRAS*, *SOS1*, *RAF1*, *SHOC2*, *HRAS*, *BRAF*, *MAPK1*, *MAP2K1*, *MAP2K2*, *MAPK3*, *SPRED1*, and *RASA1*, were evaluated for pathogenicity. Other genes were not subject to further variant analysis to avoid potential issues with incidental findings. A statistical coverage analysis was performed as described below.

Coverage analysis

Information about enrichment performance and target coverage was obtained using the software NGSrich version 0.7.8 (Frommolt *et al.*, 2012). The following parameters were measured: information about the number of reads, mean coverage, fraction of the target region with a particular depth across the 109 genes, information on the number of genes that are poorly covered, and a summary table with exon-specific coverage information at the *NF1* locus.

Direct capillary sequencing for validation

When the next-generation sequencing protocol identified truncating mutations, including nonsense mutations, frameshift mutations, and mutations at the canonical splice sites, or missense mutations that had been previously reported as being pathogenic in the literature, the variants were validated with direct capillary sequencing. In the remaining samples, all the exons were analyzed using direct capillary sequencing (Richards *et al.*, 2008). For direct capillary sequencing, 56 pairs of polymerase chain reaction (PCR) primers were designed on flanking intronic and untranslated regions to encompass the coding regions of the 58 *NF1* exons and at least 30 bp of the intronic sequence surrounding each exon (Table 2). Three primers were designed newly using primer design software, Primer3 (Rozen and Skaletsky, 2000), and the remaining primers were described elsewhere (Purandare *et al.*,

TABLE 1. LIST OF THE 109 GENES

Gene	*Chromosome*	*Basepair position (GRCh37)*	*Disease*	*Gene*	*Chromosome*	*Basepair position (GRCh37)*	*Disease*
ACTA2	10	90,694,830–90,751,146	Multisystemic smooth muscle dysfunction syndrome	*MSX1*	4	4,861,391–4,865,662	Witkop syndrome
ACTC1	15	35,080,296–35,087,926	Atrial septal defect	*MYH7*	14	23,881,946–23,904,869	Scapuloperoneal syndrome, myopathic type
ACVRL1	12	52,300,656–52,317,144	Hereditary hemorrhagic telangiectasia	*MYH9*	22	36,677,322–36,784,106	Fechtner syndrome
BRAF	7	140,415,748–140,624,563	Cardiofaciocutaneous syndrome	*NF1*	17	29,421,944–29,704,694	Neurofibromatosis type 1
CBL	11	119,076,985–119,178,858	Noonan syndrome-like disorder	*NIPBL*	5	36,876,860–37,065,925	Cornelia de Lange syndrome
CDKL5	X	18,443,724–18,671,748	Angelman syndrome-like disorder	*NOTCH2*	1	120,454,175–120,639,879	Alagille syndrome
CHD7	8	61,591,320–61,780,586	CHARGE syndrome	*NRAS*	1	115,247,084–115,259,514	Noonan syndrome
COL11A1	1	103,342,022–103,574,051	Fibrochondrogenesis	*NRTN*	19	5,823,817–5,828,334	Hirschsprung disease
COL11A2	6	33,130,468–33,160,244	Stickler syndrome	*NSD1*	5	176,560,025–176,727,213	Sotos syndrome
COL1A1	17	48,261,456–48,279,002	Osteogenesis imperfecta	*OTX2*	14	57,267,424–57,277,193	Syndromic microphthalmia
COL1A2	7	94,023,872–94,060,543	Ehlers-Danlos syndrome	*PHOX2B*	4	41,746,098–41,750,986	Congenital central hypoventilation syndrome
COL2A1	12	48,366,747–48,398,284	Stickler syndrome	*PKHD1*	6	51,480,144–51,952,422	Polycystic kidney and hepatic disease
COL3A1	2	189,839,098–189,877,471	Ehlers-Danlos syndrome	*PLOD1*	1	11,994,723–12,035,598	Ehlers-Danlos syndrome
COL5A1	9	137,533,650–137,736,688	Ehlers-Danlos syndrome	*PSPN*	19	6,375,304–6,375,859	Hirschsprung's disease
COL5A2	2	189,896,640–190,044,667	Ehlers-Danlos syndrome	*PTCH1*	9	98,205,263–98,279,246	Basal cell nevus syndrome
COL9A1	6	70,925,742–71,012,785	Stickler syndrome	*PTPN11*	12	112,856,535–112,947,716	LEOPARD syndrome
COL9A2	1	40,766,161–40,782,938	Stickler syndrome	*RAD21*	8	117,858,172–117,887,104	Cornelia de Lange syndrome
COMP	19	18,893,582–18,902,113	Epiphyseal dysplasia	*RAF1*	3	12,625,099–12,705,699	LEOPARD syndrome
CREBBP	16	3,775,054–3,930,120	Rubinstein-Taybi syndrome	*RASA1*	5	86,564,069–86,687,742	Parkes Weber syndrome
CUL7	6	43,005,354–43,021,682	3-M syndrome	*RET*	10	43,572,516–43,625,798	MENII
DCC	18	49,866,541–51,062,272	Mirror movements	*RUNX2*	6	45,296,053–45,518,818	Cleidocranial dysplasia
DDX3X	X	41,192,560–41,209,526	Medulloblastoma	*SALL1*	16	51,169,885–51,185,182	Townes–Brocks syndrome
ECE1	1	21,543,739–21,672,033	Hirschsprung disease	*SALL4*	20	50,400,550–50,419,058	Duane-radial ray syndrome
EDN3	20	57,875,498–57,901,046	Central hypoventilation syndrome	*SCN1B*	19	35,521,554–35,531,352	Brugada syndrome
EDNRB	13	78,469,615–78,549,663	Waardenburg syndrome	*SHH*	7	155,595,557–155,604,966	Holoprosencephaly
EFNB1	X	68,048,839–68,062,006	Craniofrontonasal dysplasia	*SHOC2*	10	112,679,300–112,773,424	Noonan-like syndrome
ENG	9	130,577,290–130,617,051	Heredity hemorrhagic telangiectasia	*SIX3*	2	45,169,036–45,173,215	Holoprosencephaly

(*continued*)

TABLE 1. (CONTINUED)

Gene	*Chromosome*	*Basepair position (GRCh37)*	*Disease*	*Gene*	*Chromosome*	*Basepair position (GRCh37)*	*Disease*
EP300	22	41,488,613–41,576,080	Rubinstein-Taybi syndrome	*SIX6*	14	60,975,937–60,978,524	Microphthalmia with cataract
FBN1	15	48,700,502–48,937,984	Acromicric dysplasia	*SMC1A*	X	53,401,069–53,449,676	Cornelia de Lange syndrome
FBN2	5	127,593,600–127,873,734	Congenital contractural arachnodactyly	*SMC3*	10	112,327,448–112,364,391	Cornelia de Lange syndrome
FGFR1	8	38,268,655–38,326,351	Hypogonadotropic hypogonadism	*SOS1*	2	39,208,689–39,347,685	Noonan syndrome
FGFR2	10	123,237,843–123,357,971	Antley-Bixler syndrome	*SOX10*	22	38,368,318–38,380,555	PCWH syndrome
FGFR3	4	1,795,038–1,810,598	Achondroplasia	*SOX2*	3	181,429,711–181,432,223	Syndromic microphthalmia
GDNF	5	37,812,778–37,839,781	Central hypoventilation syndrome	*SPRED1*	15	38,544,924–38,649,449	Legius syndrome
GFRA1	10	117,816,435–118,033,125	Hirschsprung's disease	*SPRY2*	13	80,910,110–80,915,085	Holoprosencephaly
GFRA2	8	21,549,529–21,672,391	Hirschsprung's disease	*STAG1*	3	136,055,077–136,471,220	Cornelia de Lange syndrome
GLA	X	100,652,778–100,663,000	Fabry disease	*TAZ*	X	153,639,876–153,650,064	Barth syndrome
HRAS	11	532,241–535,560	Costello syndrome	*TBX22*	X	79,270,254–79,287,267	Abruzzo-Erickson syndrome
IHH	2	219,919,141–219,925,237	Acrocapitofemoral dysplasia	*TBX5*	12	114,791,734–114,846,246	Holt-Oram syndrome
IRF6	1	209,958,967–209,979,519	Van der Woude syndrome	*TCF4*	18	52,889,561–53,303,251	Pitt-Hopkins syndrome
JAG1	20	10,618,331–10,654,693	Alagille syndrome	*TCOF1*	5	149,737,201–149,779,870	Treacher Collins syndrome
KCNE1	21	35,790,909–35,884,572	Jervell and Lange-Nielsen syndrome	*TGFBR1*	9	101,867,411–101,916,473	Loeys-Dietz syndrome
KCNJ2	17	68,164,756–68,176,188	Andersen syndrome	*TGFBR2*	3	30,647,993–30,735,633	Loeys-Dietz syndrome
KCNQ1	11	2,466,220–2,870,339	Jervell and Lange-Nielsen syndrome	*TGIF1*	18	3,411,924–3,458,408	Holoprosencephaly
KIAA1279	10	70,748,476–70,776,738	Goldberg-Shprintzen megacolon syndrome	*TP63*	3	189,348,941–189,615,067	EEC syndrome
KIF26A	14	104,605,059–104,647,234	Megacolon	*TRAPPC10*	21	45,432,205–45,526,432	Holoprosencephaly
KRAS	12	25,358,179–25,403,869	Noonan syndrome	*TRIM37*	17	57,059,998–57,184,265	Mulibrey nanism
L1CAM	X	153,126,968–153,151,627	CRASH syndrome	*TSC1*	9	135,766,734–135,820,093	Tuberous sclerosis
LAMP2	X	119,560,002–119,603,203	Danon disease	*TSC2*	16	2,097,471–2,138,712	Tuberous sclerosis
MAP2K1	15	66,679,181–66,783,881	Cardiofaciocutaneous syndrome	*TWIST1*	7	19,039,314–19,157,294	Saethre Chotzen syndrome
MAP2K2	19	4,090,318–4,124,125	Cardiofaciocutaneous syndrome	*VHL*	3	10,183,318–10,195,353	Von Hippel-Lindau syndrome
MAPK1	22	22,113,945–22,221,969	Acromesomelic dysplasia	*VSX2*	14	74,706,174–74,729,440	Microphthalmia
MAPK3	16	30,125,425–30,134,629	Cardiac hypertrophy	*ZEB2*	2	145,141,941–145,277,957	Mowat-Wilson syndrome
MECP2	X	153,287,024–153,363,187	Rett syndrome	*ZIC2*	13	100,634,025–100,639,018	Holoprosencephaly
MID1	X	10,413,349–10,851,828	Opitz GBBB syndrome				

Table 2. List of Polymerase Chain Reaction Primers

Exon	Primer sequence (5′-3′)	Amplicon size	Reference	Exon	Primer sequence (5′-3′)	Amplicon size	Reference
1	CAGACCCTCTCCTTGCCTCTT GGATGGAGGGTCGGAGGCTG	439	Purandare *et al.* (1995)	29	ATATGGAGCAGGTATAATAAAC AAAACAGCGGTTCTATGTG	181	Bausch *et al.* (2007)
2	CGTCATGATTTTCAATGGCAAG GCTCACTGAATCTAAAACCCAGC	438	Bausch *et al.* (2007)	30	CGTTGCACTTGGCTTAATGTCTG CCATCAGCAGCTAGATCCTTCTTT	327	Bausch *et al.* (2007)
3	TTTCACTTTTCAGATGTGTGTTG TGGTCCACATCTGTACTTTG	245	Purandare *et al.* (1995)	31	TTTTCTGTGATTCATAGCC GATATTCTTAACAAACAGCA	400	This report
4	TTAAATCTAGGTGGTGTGT AAACTCATTTCTCTGGAG	517	Han *et al.* (2001)	32	CTTATACTCAATTCTCAACTCC GAATTTAAGATAGCTAGATTATC	226	Bausch *et al.* (2007)
5	GAGATACCACACCTGTCCCCTAA TTGACCCAGTGATTTTTTTCAGA	215	Bausch *et al.* (2007)	33	GACTTCATACAATAAATAATCTG TATTTGATTCAAACAGAGCAAC	195	Bausch *et al.* (2007)
6	TTTCCTAGCAGACAACTATCGA AGGATGCTAACAACAGCAAAT	308	Han *et al.* (2001)	34	CTCCATATTTGTAATCTTAGTTA GGAGAGTGTTCACTATCCC	298	Bausch *et al.* (2007)
7	GAAGGAAGTTAGAAGTTTGTG CACAAGTAGGCATTTAAAAGA	211	Bausch *et al.* (2007)	35	GTTACAAGTTAAAGAAATGTGTAG CTAACAAGTGGCCTGGTGGCAAAC	298	Purandare *et al.* (1995)
8	CATGTTTATCTTTTAAAAATGTTGCC ATAATGGAAATAATTTTGCCCTCC	301	Han *et al.* (2001)	36	TTTATTGTTTATCCAATTATAGACTT TCCTGTTAAGTCAACTGGGAAAAAC	296	Purandare *et al.* (1995)
9	CTGTTAATTTGCTATAATATTAGC CATAATACTTATGCTAGAAAATTC	328	Bausch *et al.* (2007)	37	TGAATCCAGACTTTGAAGAATTGTT CTAGGGAGGCCAGGATATAGTCTAGT	644	Bausch *et al.* (2007)
10	GTAATGTGTTGATGTTATTACATG GTCTTTTTGTTTATAAAGGATAACA	273	Bausch *et al.* (2007)	38	GGTTGGTTTCTGGAGCCTTTTAGA CAACAAACCCCAAATCAAACTGA	467	Bausch *et al.* (2007)
11	CTTTCTATTTGCTGTTCTTTTTGG CCTTTTTGAAAACCAAGAGTGCA	264	Bausch *et al.* (2007)	39	TTGGAACTATAAGGAAAAATACGTTT AGGGTTTTCTTTGAATTCTCTTAGA	321	Bausch *et al.* (2007)
12	ACGTAATTTTGTACTTTTTCTTCC CAATAGAAAGGAGGTGAGATTC	222	Purandare *et al.* (1995)	40	ATAATTGTTGATGTGATTTTCATTG AATTTTGAACCAGATGAAGAG	424	Han *et al.* (2001)
13	GCAAAAACGATTTTCATTGTTTTGT GCGTTTCAGCTAAACCCAATT	403	This report	41	TTGATTAGGCTGTTCCAATGAA CAAAACAAAAAACCTCCTGATGAT	298	Bausch *et al.* (2007)
14	ATTGAAGTTTCCTTTTTTTCCTTG GTATAGACATAAACATACCATTTC	275	Bausch *et al.* (2007)	42	GTGCTAAAACTTTGAGTCCCATGT ATAATCTATATTGATCAGGTGAAGTA	415	Bausch *et al.* (2007)
15	CCAAAAATGTTTGAGTGAGTCT ACCATAAAACCTTTGGAAGTG	256	Han *et al.* (2001)	43	GCAAGGAGCATTAATACAATGTATC CCATGCAAGTGTTTTTATTTAAGC	507	Bausch *et al.* (2007)

(*continued*)

TABLE 2. (CONTINUED)

Exon	*Primer sequence (5′-3′)*	*Amplicon size*	*Reference*	*Exon*	*Primer sequence (5′-3′)*	*Amplicon size*	*Reference*
16	AAACCTTACAAGAAAAACTAAGCT ATTACCATTCCAAATATTCTTCCA	303	Purandare *et al.* (1995)	44–45	GGTAACAGGTCACTTAATGACATCA GACCTCAAATTTAAACGTCTTTTAGA	512	Bausch *et al.* (2007)
17	CTCTTGGTTGTCAGTGCTTC CAGAAAACAAACAGAGCACAT	261	Han *et al.* (2001)	46	CATTCCGAGATTCAGTTTAGGAG AAGTAACATTCAACACTGATACCC	236	Abernathy *et al.* (1997)
18	CCCAAGTTGCAAATATATGTC GTGCTTTGAGGCAGACTGAG	336	Bausch *et al.* (2007)	47	TCCCCAAAAGAGAAAACATGG AGCAACAAGAAAAGATGGAAGAGT	334	Bausch *et al.* (2007)
19	TGAAGCATTTGCTCTGCTCT GTTTCAAACTTGATGTATATTAAA	347	Bausch *et al.* (2007)	48	CTACTGTGTGAACCTCATCAACC GTAAGACATAAGGGCTAACTTACTTC	284	Abernathy *et al.* (1997)
20	ACTTGGCTGTAGCTGATTGA ACTTTACTGAGCGACTCTTGAA	247	Han *et al.* (2001)	49	TCAGGGAAGAAGACCTCAGCAGATGC TGAACTTTCTGCTCTGCCACGCAACC	328	Abernathy *et al.* (1997)
21	GGAAGAAATGTTGGATAAAGCA AAACAAGTCACTCTATTCATAGA	579	Bausch *et al.* (2007)	50	GTGCACATTTAACAGGTACTAT CTTCCTAGGCCATCTCTAGAT	373	Han *et al.* (2001)
22	TATCTGTATGCTTATTTGGCTCTA GTGCAGTAAAGAATGGCCAG	385	Bausch *et al.* (2007)	51	CTTGGAAGGAGCAAACGATGGTTG CAAAAACTTTGCTACACTGACATGG	356	Abernathy *et al.* (1997)
23	AGAAGTTGTGTACGTTCTTTTCT CTCCTTTCTACCAATAACCGC	367	Purandare *et al.* (1995)	52	GCTCCAGGGATGTATTAGAGCTTT TGACTTTCATGTACTCTCCCACCT	325	Bausch *et al.* (2007)
24	TTGTTCCCTTCTGGCTTTTAT ATCTCAAAAGTTTAAATACACA	365	This report	53–54	TGAAGTGATTATCCAGGTGTTTGA AAAGACAGGCACGAAGGTGA	506	Bausch *et al.* (2007)
25	TGAGGGGAAGTGAAAGAACT GGCTTTATTTGCTTTTTGCT	235	Han *et al.* (2001)	55	AATTTTGGCACATTATTCTGGG AGCAAGTTCATCAACCATCCTT	290	Bausch *et al.* (2007)
26	CCACCCTGGCTGATTATCG TAATTTTTGCTTCTCTTACATGC	402	Purandare *et al.* (1995)	56	CTGTTACAATTAAAAGATACCTTGC TGTGTGTTCTTAAAGCAGGCATAC	185	Abernathy *et al.* (1997)
27	TGGTCTCATGCACTCCATA CATCTTTCTTCTGGCTCTGA	474	Han *et al.* (2001)	57	TTTTGGCTTCAGATGGGGATTTAC AAGGGAATTCCTAATGTTGGTGTC	351	Abernathy *et al.* (1997)
28	TGCTACTCTTTAGCTTCCTAC CCTTAAAAGAAGACAATCAGCC	331	Purandare *et al.* (1995)	58	AAGCGACACATGACTGCAATG TGGCTTTCATCACTGGCCA	571	Bausch *et al.* (2007)

1995; Abernathy *et al.*, 1997; Han *et al.*, 2001; Bausch *et al.*, 2007). The 3′ end of the primers were designed so as not to match the genomic sequences of any of the highly homologous pseudogene sequences to avoid mispriming to the pseudogenes. Direct capillary sequencing was performed using the ABI BigDye version 1.1 Terminator Cycle Kit (Life Technologies) and the ABI Prism 3500 Capillary Array Sequencer (Life Technologies). The sequence data were analyzed using Mutation Surveyor version 4.0.6 (Softgenetics) and Sequencher version 5.0 (Gene Codes Corp.).

Multiplex ligation-dependent probe amplification

When the next-generation sequencing protocol did not identify truncating mutations, canonical splice-site mutations, or other point mutations previously reported as pathological missense change or splicing defect, the remaining samples were screened for single/multiple exon deletions or duplications using a multiplex ligation-dependent probe amplification method (De Luca *et al.*, 2007) (SALSA P081/082-B2 NF1 MLPA assay kit; MRC-Holland) concurrently with the direct capillary sequencing of all the exons, as stated above.

Analysis algorithm of the variants

Missense variants that have not been reported as pathogenic in the literature and were not observed in the 1208 normal Japanese exome data were evaluated for potential pathogenicity using five bioinformatics programs, including SIFT (Kumar *et al.*, 2009), Polyphen2 (Adzhubei *et al.*, 2010), LRT (Chun and Fay, 2009), MutationTaster (Schwarz *et al.*, 2010), and PhyloP (Siepel *et al.*, 2009). When four of the five programs predicted the results as pathogenic ("damaging" with SIFT, "probably damaging" with PolyPhen2, "deleterious" with LRT, "disease causing" with MutationTaster, or "conserved" with PhyloP), we interpreted the clinical significance of the missense mutation as being putatively pathogenic.

Results

Performance of sequence capturing

In the custom-designed mutation analysis panel for the screening of classic genetic syndromes, the number of bases for targeted capturing was 459,952 bp over 1888 regions of the 109 target genes, including *NF1*. An average of 207,203 reads per sample were mapped and aligned uniquely to the targeted bases of the 109 genes among the 86 samples.

As far as the *NF1* locus was concerned, all the exons were highly covered with a coverage of 190.7x per sample. Overall, 99.3% of the regions were covered at least with a coverage of 5x and 98.8% of the regions were covered at least with a coverage of 30x. The mean coverage of all the exons in the 86 samples indicated that all the exons, but exon 1, were appropriate for base calling by next-generation sequencing (Table 3). Because of the poor coverage, exon 1 was sequenced using the direct capillary sequencing in all 86 samples, none of which had any variants.

The mean coverage over the entire targeted regions per sample was 131.0x, and most of the regions were well covered (Table 4). Overall, 97.1% of the regions were covered at least 5x coverage, and 84.4% of the regions were covered at least 30x coverage. Some exons of *NF1* and other regions were less well covered than others. Exon 15 and exon 50 of *NF1*, together with the *COMP* gene and the *PHOX2B* gene, had relatively low coverages of 86.9x, 79.1x, 55.3x, and 19.2x, respectively.

TABLE 3. MEAN COVERAGE OF *NF1* EXONS AMONG 86 PATIENTS

Exon	*Coverage (x)*	*Exon*	*Coverage (x)*
1	1.7	30	239.7
2	220.2	31	175.9
3	168.8	32	157.0
4	169.5	33	124.6
5	145.0	34	216.0
6	170.9	35	152.1
7	164.8	36	189.3
8	144.0	37	284.7
9	182.7	38	261.5
10	174.1	39	230.9
11	179.2	40	217.3
12	194.9	41	206.8
13	120.0	42	276.9
14	141.2	43	195.7
15	86.9	44	181.1
16	152.7	45	166.3
17	212.6	46	156.4
18	251.3	47	185.7
19	127.1	48	159.4
20	215.4	49	241.5
21	175.2	50	79.1
22	191.4	51	174.3
23	103.1	52	238.4
24	194.0	53	235.9
25	96.6	54	217.5
26	212.1	55	136.8
27	209.6	56	320.0
28	238.7	57	220.5
29	208.5	58	122.6

NF1 has seven highly homologous pseudogene sequences located in chromosomes other than chromosome 17 (2q12-q13, 12q11, 14p11-q11, 15q11.2, 18p11.2, 21p11-q11, and 22p11-q11), on which *NF1* resides (Upaddhyaya, 2008). We scrutinized the mapped reads among 10 arbitrarily selected patients; all the pseudogene sequences were mapped to their orthologous locations in the genome rather than the *NF1* locus on chromosome 17.

Coverage of the 108 genes other than the *NF1* gene was evaluated in all 86 samples. The mean coverage of all 108 genes on the same diagnostic panel indicated that the mean coverage ranged from 19.2x to 254.1x, with mean of 114.5x (Table 4).

Mutation detection

The next-generation sequencing protocol described above led to the identification of pathological *NF1* mutations in 70 of the 86 patients who met the NIH diagnostic criteria. The clinical information is listed in Table 5. All the 70 patients harbored mutations in a heterozygous state: 30 nonsense mutations, 19 frameshift mutations, 8 canonical splice-site mutations, and 6 point mutations that were previously reported and have been shown to lead to aberrant splicing

TABLE 4. SUMMARY OF THE COVERAGE OF 109 GENES

Gene	*Coverage (x)*	*Gene*	*Coverage (x)*
ACTA2	103.7	*MSX1*	49.4
ACTC1	111.4	*MYH7*	103.5
ACVRL1	60.4	*MYH9*	97.5
BRAF	160.0	*NF1*	190.7
CBL	192.3	*NIPBL*	175.9
CDKL5	146.1	*NOTCH2*	153.4
CHD7	150.6	*NRAS*	254.1
COL11A1	160.5	*NRTN*	45.8
COL11A2	66.8	*NSD1*	160.1
COL1A1	47.2	*OTX2*	115.1
COL1A2	127.0	*PHOX2B*	19.2
COL2A1	76.2	*PKHD1*	173.6
COL3A1	123.1	*PLOD1*	68.3
COL5A1	52.0	*PSPN*	66.5
COL5A2	159.2	*PTCH1*	111.0
COL9A1	147.4	*PTPN11*	152.6
COL9A2	52.4	*RAD21*	198.5
COMP	55.3	*RAF1*	154.9
CREBBP	50.1	*RASA1*	171.7
CUL7	68.8	*RET*	97.4
DCC	188.4	*RUNX2*	144.5
DDX3X	118.1	*SALL1*	91.7
ECE1	80.6	*SALL4*	93.8
EDN3	64.6	*SCN1B*	69.3
EDNRB	178.9	*SHH*	50.3
EFNB1	47.8	*SHOC2*	195.5
ENG	36.4	*SIX3*	80.0
EP300	191.0	*SIX6*	67.6
FBN1	177.2	*SMC1A*	134.7
FBN2	171.0	*SMC3*	157.2
FGFR1	102.7	*SOS1*	180.5
FGFR2	157.5	*SOX10*	45.1
FGFR3	34.8	*SOX2-OT*	89.0
GDNF	200.5	*SPRED1*	137.0
GFRA1	103.1	*SPRY2*	141.7
GFRA2	49.9	*STAG1*	193.3
GLA	121.1	*TAZ*	45.1
HRAS	44.4	*TBX22*	117.7
IHH	73.4	*TBX5*	124.2
IRF6	128.5	*TCF4*	170.8
JAG1	147.5	*TCOF1*	68.4
KCNE1	88.4	*TGFBR1*	190.0
KCNJ2	226.4	*TGFBR2*	89.6
KCNQ1	80.5	*TGIF1*	77.1
KIAA1279	186.5	*TP63*	182.5
KIF26A	33.7	*TRAPPC10*	139.7
KRAS	214.4	*TRIM37*	85.4
L1CAM	42.7	*TSC1*	157.8
LAMP2	128.2	*TSC2*	49.4
MAP2K1	151.4	*TWIST1*	47.9
MAP2K2	35.6	*VHL*	84.5
MAPK1	168.5	*VSX2*	29.7
MAPK3	87.1	*ZEB2*	218.9
MECP2	80.4	*ZIC2*	72.9
MID1	126.4		

according to reverse transcription (RT)-PCR studies, together with seven nonsynonymous substitutions (Table 5). Among the seven nonsynonymous substitutions, four were previously reported to be pathogenic based on functional assays or the inheritance pattern within the families (Li *et al.*, 1992; Fahsold *et al.*, 2000; Lee *et al.*, 2006).

Three samples with missense mutations that have never been reported in the literature were predicted to be pathogenic based on the consensus predication from multiple bioinformatics programs. Five programs, including SIFT, Polyphen2, LRT, Mutation Taster, and PhyloP, predicted potential pathogenicity as follows: c.2183T>G (p.Val728Gly) mutation was predicted to be pathogenic by all five programs, and c.2540T>G (p.Leu847Arg) and c.6818A>T (p.Lys2273Met) mutations were predicted to be pathogenic by four of the five bioinformatics programs. None of the three missense mutations resided within the critical functional domain, GAP-related domain that regulates the RasGAP activity.

Comparison of the distributions of nonsense, splice-site variants, and missense mutations in the Japanese population versus the northern European population, as reported by Messiaen *et al.* (2000), Nemethova *et al.* (2013), Sabbagh *et al.* (2013), and Valero *et al.* (2011), revealed no statistically significant differences among the groups ($p=0.203$ using the Fisher exact test for countable data).

Together with these 3 samples, which were subject to bioinformatics programs, 16 samples without truncating mutations or missense mutations, previously reported to be pathogenic, were further sequenced using direct capillary sequencing methods. All the exons were sequenced, including exon 1, and no additional point mutations or small indels were detected. These 19 patients were further screened for relatively large deletions that would span an entire exon or multiple exons and thus escape from direct capillary sequencing. Among 10 patients, 5 were shown to have a whole *NF1* deletion, 2 had multiple-exon deletions, and 3 had single-exon deletions. These five patients with a whole *NF1* deletion were apparently homozygous for all the SNPs for the entire *NF1* region according to the next-generation sequencing analysis.

Overall, no appreciable genotype–phenotype correlation was detected in the present study (Table 5). Variants were detected in genes other than *NF1* when the same criteria used in the *NF1* analysis were applied to these genes (Table 5). None of these variants was classified as truncating mutations and none of them listed in the Human Genome Mutation Database (HGMD) (Cooper *et al.*, 1998). Such rare variants of unknown significance among the genes on the panel were found in at least two-thirds of the patients. Patients with variants in genes other than *NF1* did not necessarily exhibit a severe *NF1* phenotype.

Discussion

The present study demonstrated that next-generation sequencing with in-solution hybridization-based enrichment provides a high mutation detection rate comparable to that of conventional direct capillary sequencing methods for the molecular diagnosis of neurofibromatosis. The overall mutation detection rate using the currently reported method in 86 patients who met the clinical diagnostic criteria was 81.4% (70/86). Among the 16 samples in which mutations were not detected using next-generation sequencing, 10 samples were later shown to have large deletions using a different method, multiplex ligation-dependent probe amplification (MLPA). Because of their large sizes, the 10 large deletions would not have been detected using the direct capillary sequencing

TABLE 5. SUMMARY OF PATHOGENIC MUTATIONS DETECTED BY NEXT-GENERATION SEQUENCING

Exon	*Genomic mutation*	*Amino acid substitution*	*Type of mutation*	*Reference*	*Age*	*Familial*	*Symptoms*	*Variations of unknown significance in rasopathy genes*	*Number of mutations in other genes*
2	c.83_84insG	p.Asn29Glufs*9	Frameshift		68	Yes	P,N	RASA1 c.293C>T p.Ala98Val	2
3	c.264_265insA	p.Thr89Asnfs*18	Frameshift		44	Yes	P,B,N		1
5	c.491T>A	p.Leu164*	Nonsense		50	Yes	P,B,O,N		1
5	c.495-498delTGTT	p.Cys167Glnfs*10	Frameshift		41	No	P,N,L		1
5	c.499_500insG	p.Cys167Trpfs*7	Frameshift		27	No	P,B,N,L		1
5	c.574C>T	p.Arg192*	Nonsense		32	No	P,N,L		2
10	c.1105C>T	p.Gln369*	Nonsense		40	Yes	P,N,L		1
11	c.1241T>G	p.Leu414Arg	Missense[a]	Lee *et al.* (2006)	21	No	P,N,L		1
11	c.1246C>T	p.Arg416*	Nonsense		32	Yes	P,B,N		1
12	c.1381C>T	p.Arg461*	Nonsense		3	No	P	RASA1 c.669G>C p.Gln223His	1
12	c.1381C>T	p.Arg461*	Nonsense		67	Yes	P,B,N		1
12	c.1381C>T	p.Arg461*	Nonsense		41	Yes	P,B,N		0
13	c.1466A>G	p.Tyr489Cys	Missense[a]	Messiaen *et al.* (2000)	36	No	P,N		1
13	c.1466A>G	p.Tyr489Cys	Missense[a]	Messiaen *et al.* (2000)	63	Yes	P,B,N		0
13	c.1466A>G	p.Tyr489Cys	Missense[a]	Messiaen *et al.* (2000)	71	No	P,N,L		1
13	c.1527+1_+4delGTAA		Splicing		30	No	P,N,L		2
14	c.1541_1542delAG	p.Gln514Argfs*43	Frameshift		52	No	P,B,N		1
15	c.1721+3A>G		Splicing	Purandare *et al.* (1994)	40	Yes	P,B,N		0
16	c.1726C>T	p.Gln576*	Nonsense		36	No	P,N		0
16	c.1754_1757delACTA	p.Thr586Valfs*18	Frameshift		49	Yes	P,N		0
16	c.1765C<T	p.Gln589*	Nonsense		40	No	P,N		1
16	c.1832delT	p.Asn614Ilefs*17	Frameshift		80	No	P,N,L		3
17	c.1876_1877insT	p.Tyr628Leufs*6	Frameshift		79	Yes	P,B,N,L		2
17	c.1885G>A	p.Gly629Arg	Missense[a]	Gasparini *et al.* (1996)	57	Yes	P,N		2
18	c.2041C>T	p.Arg681*	Nonsense		23	No	P,N		1
18	c.2041C>T	p.Arg681*	Nonsense		35	Yes	P,B,N		1
18	c.2087G>A	p.Trp696*	Nonsense		58	Yes	P,B,N,L		0
18[b]	c.2183T>G	p.Val728Gly	Missense		67	Yes	P,N		0
21	c.2423delT	p.His809Thrfs*12	Frameshift		43	Yes	P,N		1
21	c.2540T>C	p.Leu847Pro	Missense[a]	Fahsold *et al.* (2000)	33	Yes	P,N,L		0
21	c.2540T>C	p.Leu847Pro	Missense[a]	Fahsold *et al.* (2000)	59	Yes	P,B,N,L		0

(*continued*)

TABLE 5. (CONTINUED)

Exon	*Genomic mutation*	*Amino acid substitution*	*Type of mutation*	*Reference*	*Age*	*Familial*	*Symptoms*	*Variations of unknown significance in rasopathy genes*	*Number of mutations in other genes*
21[b]	c.2540T>G	p.Leu847Arg	Missense		55	No	P,N		0
21	c.2446C>T	p.Arg816*	Nonsense		52	Yes	P,N,L		0
22	c.2851-5_-2delTTTA		Splicing		19	No	P,B,N,L		1
23	c.3048T>A	p.Cys1016*	Nonsense		50	Yes	P,B,N		0
24	c.3132C>A	p.Tyr1044*	Nonsense		12	Yes	P,O,N		0
25	c.3213_3214delAA	p.Ser1072Hisfs*16	Frameshift		29	No	P,N,L		2
27	c.3595_3596insGG	p.Thr1199Argfs*17	Frameshift		20	No	P,N,L		1
27	c.3615_3616delTG	p.Phe1205Leufs*12	Frameshift		37	Yes	P,B,N		2
27	c.3615_3616delTG	p.Phe1205Leufs*12	Frameshift		64	Yes	P,B,N,L		1
28	c.3709-2A>G		Splicing		44	No	P,B,N,L		0
28	c.3765_3766insCT	p.Leu1257Cysfs*10	Frameshift		29	No	P,B,N,L		2
28	c.3826C>T	p.Arg1276*	Nonsense		21	No	P,O,B,N,L		0
29	c.3888T>A	p.Tyr1296*	Nonsense		49	No	P,N,L		0
30	c.4084C>T	p.Arg1362*	Nonsense		27	No	P,N		1
32	c.4329delA	p.Lys1444Argfs*25	Frameshift		50	Yes	P,B,N,L		0
32	c.4330A>G	p.Lys1440Glu	Missense[a]	Li *et al.* (1992)	40	No	P,N,L		0
33	c.4430+1G>A		Splicing		49	Yes	P,B,N		2
34	c.4544delA	p.Gln1515Argfs*59	Frameshift		35	Yes	P,N		2
35	c.4716_4724+6 delTATGACTAGGTAAAG		Splicing		50	No	P,B,N,L		1
36	c.4743_4744delAG	p.Glu1582Argfs*39	Frameshift		36	No	P,B,N,L		2
36	c.4769T>G	p.Leu1590*	Nonsense		45	No	P,N		1
37	c.4873_4874insA	p.Tyr1625*	Nonsense		63	No	P,B,N		1
37	c.5198T>G	p.Leu1733*	Nonsense		40	No	P,B,N,L		1
38	c.5269-6_5276 delTTCCAGGTTGGTTC		Splicing		38	No	P,N,L		1
38	c.5269-1G>A		Splicing		39	Yes	P,B,N,L		0
38	c.5516_5517insC	p.Glu1841Profs*21	Frameshift		31	Yes	P,B,N		1
38	c.5609G>A	p.Arg1870Gln	Missense[a]	Ars *et al.* (2003)	69	Yes	P,B,N		0
40	c.5902C>T	p.Arg1968*	Nonsense		22	No	P,N		1
44	c.6675G>A	p.Trp2225*	Nonsense		54	No	P,O,B,N		3
45	c.6772C>T	p.Arg2258*	Nonsense		69	Yes	P,N		0
45	c.6772C>T	p.Arg2258*	Nonsense		52	Yes	P,B,N,L		1
45[b]	c.6818A>T	p.Lys2273Met	Missense		46	No	P,N		1

(*continued*)

TABLE 5. (CONTINUED)

Exon	*Genomic mutation*	*Amino acid substitution*	*Type of mutation*	*Reference*	*Age*	*Familial*	*Symptoms*	*Variations of unknown significance in rasopathy genes*	*Number of mutations in other genes*
46	c.6850_6853delACTT	p.Tyr2285Thrfs*5	Frameshift		42	Yes	P,N		1
46	c.6853_6854insA	p.Tyr2285*	Nonsense		21	No	P,N		0
46	c.6853_6854insA	p.Tyr2285*	Nonsense		28	No	P,N		0
46	c.6904C>T	p.Gln2302*	Nonsense		37	Yes	P,N,L		1
47	c.6950G>A	p.Trp2317*	Nonsense		25	No	P,B,N,L		0
50	c.7348C>T	p.Arg2450*	Nonsense		46	No	P,B,N,L		0
54	c.7970+1_+4delGTAA		Splicing		41	Yes	P,N,L		2
			ex1 to 58 deletion		13	No	P,N,L		3
			ex1 to 58 deletion		29	No	P,N		1
			ex1 to 58 deletion		68	No	P,N		1
			ex1 to 58 deletion		58	No	P,B,N,L		1
			ex1 to 58 deletion		34	No	P,B,N		1
			ex1 deletion		68	No	P,N,L		1
			ex3 to 4 deletion		59	No	P,N,L		0
			ex6 to 51 deletion		36	Yes	P,N,L		2
			ex8 deletion		28	Yes	P,N		0
			ex12 deletion		55	No	P,N		1
					37	No	P		0
					50	No	P,N		0
					45	Yes	P,N,L		2
					30	No	P,N		0
					34	Yes	P,B,N		1
					25	No	P		0

[a]Previously reported to cause aberrant splicing.
[b]Predicted to be pathogenic by bioinformatics programs.
Symptoms: P, pigment; O, optic nerve tumor; B, bone manifestation; N, neurofibroma; L, Lisch nodules; HGMD; Human Genome Mutation Database.

method, which is currently considered to be the gold standard. The mutation detection rate was 92.1% (70/76) when these 10 samples were excluded from the calculation of the detection rate.

Among the 10 samples with large deletions, 5 patients with a whole *NF1* deletion could have been suspected of having a whole gene deletion, in that these patients were apparently homozygous for all the SNPs for the entire *NF1* region according to the next-generation sequencing data. The remaining five patients with a partial deletion of the *NF1* gene, as documented using MLPA, would not have been reliably inferred to have such a deletion based on the relatively short runs of homozygosity.

Recent reports on comprehensive *NF1* screening using the direct capillary sequencing method revealed that the detection rate was 89.5–96.3% when cases with large deletions detectable only by using MLPA were excluded [93.4%: Valero *et al.* (2011), 89.5%: Nemethova *et al.* (2013), 96.3%: Sabbagh *et al.* (2013)]. Hence, the performance of the presently reported protocol was comparable with that of the direct capillary sequencing methods.

The present protocol uses genomic DNA as the starting material, unlike other protocols using puromycin-tested Epstein-Barr virus cell lines as the starting material for RT-PCR (Messiaen *et al.*, 2000). Apparently, the use of genomic DNA is much easier in clinical settings. Yet, genetic testing based on genomic DNA, including the previously reported protocol, cannot predict potential splicing defects caused by point mutations. The use of RNA would be more sensitive to splicing abnormalities, if any, because of the possibility of mutations located deep in the intron or aberrant splicing defects caused by point mutations within coding sequences that were not evaluated in the presently reported protocol. However, such deep intronic mutations or splicing defects may be relatively rare, given the high overall detection rate of 92.1% in the present study.

The mean coverage of the entire target regions per sample was 131.0x. This coverage figure was considered to be sufficient for the detection of heterozygous base changes. Furthermore, the observation that rare variants in some genes on the panel were found in at least two-thirds of the patients supports the notion that the diagnostic performance of the panel for other genes is as robust as it is for *NF1*. Thus, our results regarding the validity of next-generation sequencing for the molecular diagnosis of the *NF1* gene, in comparison with direct capillary sequencing, can be extrapolated to the molecular diagnosis of other classic malformation syndromes.

Nevertheless, exon-to-exon variations in the coverage figures should be carefully evaluated. The extremely low coverage of the *NF1* exon1 can be ascribed to its extremely high GC content of 77.5%, in that a GC content of 60% or higher is associated with a sharp decrease in the read depth (Chilamakuri *et al.*, 2014). Similarly, a relatively low coverage of the *COMP* gene of 55.3x may be associated with a GC content of 63.4%. Exon 15 and exon 50 of *NF1*, together with the *PHOX2B* gene, had relatively low coverages of 86.9x, 79.1x, and 19.2x, respectively. The underlying cause of such variations is currently unexplained in that the GC contents of these regions were 32.2%, 39.4%, and 54.5%, respectively.

We estimated that the cost for consumables would be about USD 400 for direct capillary sequencing of the *NF1* gene, excluding labor costs. The estimated cost for consumables for the NGS panel analysis would be comparable. Hence, if we were to screen for the single *NF1* gene, the cost–benefit of next-generation sequencing may not be advantageous. However, if we were to screen for genes associated with conditions to be differentiated from neurofibromatosis using direct capillary sequencing, the consumable cost would be multiplied, whereas the cost for the screening of extra genes using next-generation sequencing would remain fixed. Indeed, the molecular diagnosis of Legius syndrome and Noonan syndrome would be helpful for the clinical management and outcome predictions of patients with café-au-lait spots, since patients with these conditions are unlikely to develop neurofibromas or other hamartomatous complications.

The availability of a mutation analysis panel, like the one presented herein, plays a critical role in differentiating the underlying genetic cause of patients whose diagnosis is uncertain from a clinical standpoint (Takenouchi *et al.*, 2013a, 2013b). The use of a whole-exome panel would be advantageous because of its comprehensiveness. However, apart from the higher cost of a whole-exome analysis, a panel approach enables a higher sensitivity (Chin *et al.*, 2013) because the average coverage, and thus the sensitivity, is higher using a panel approach (close to 100%) compared with a whole-exome approach (85%–95%).

Acknowledgments

All the authors would like to express their sincere appreciation to Mr. Yuji Sugie for his special support and all the patients and their families who were enrolled in this study. This work was partly supported by Research on Applying Health Technology and Research on Rare and Intractable Diseases from the Ministry of Health, Labour and Welfare, Japan.

Author Disclosure Statement

The authors declare that they have no competing interests.

References

Abernathy CR, Rasmussen SA, Stalker HJ, *et al.* (1997) *NF1* mutation analysis using a combined heteroduplex/SSCP approach. Hum Mutat 9:548–554.

Adzhubei IA, Schmidt S, Peshkin L, *et al.* (2010) A method and server for predicting damaging missense mutations. Nat Methods 7:248–249.

Aoki Y, Niihori T, Narumi Y, *et al.* (2008) The RAS/MAPK syndromes: novel roles of the RAS pathway in human genetic disorders. Hum Mutat 29:992–1006.

Aramaki M, Udaka T, Torii C, *et al.* (2006) Screening for CHARGE syndrome mutations in the *CHD7* gene using denaturing high-performance liquid chromatography. Genet Test Mol Biomarkers 10:244–251.

Ars E, Kruyer H, Morell M, *et al.* (2003) Recurrent mutations in the *NF1* gene are common among neurofibromatosis type 1 patients. J Med Genet 40:e82.

Bausch B, Borozdin W, Mautner VF, *et al.* (2007) Germline *NF1* mutational spectra and loss-of-heterozygosity analyses in patients with pheochromocytoma and neurofibromatosis type 1. J Clin Endocrinol Metab 92:2784–2792.

Carey JC, Viskochil DH (1999) Neurofibromatosis type 1: A model condition for the study of the molecular basis of variable expressivity in human disorders. Am J Med Genet 89:7–13.

Chilamakuri CS, Lorenz S, Madoui MA, *et al.* (2014) Performance comparison of four exome capture systems for deep sequencing. BMC Genomics 15:449.

Chin E, Zhang V, Wang J, *et al.* (2013) Frequently asked questions about the clinical utility of next-generation sequencing in molecular diagnosis of human genetic diseases. In: Wong L-JC (ed) Next Generation Sequencing: Translation to Clinical Diagnostics. Springer Science+Business Media, New York, pp 287–299.

Chun S, Fay JC (2009) Identification of deleterious mutations within three human genomes. Genome Res 19:1553–1561.

Cingolani P, Platts A, Wang le L, *et al.* (2012) A program for annotating and predicting the effects of single nucleotide polymorphisms, SnpEff: SNPs in the genome of Drosophila melanogaster strain w^{1118}; iso-2; iso-3. Fly 6:80–92.

Cooper DN, Ball EV, Krawczak M (1998) The human gene mutation database. Nucleic Acids Res 26:285–287.

De Luca A, Bottillo I, Dasdia MC, *et al.* (2007) Deletions of *NF1* gene and exons detected by multiplex ligation-dependent probe amplification. J Med Genet 44:800–808.

Fahsold R, Hoffmeyer S, Mischung C, *et al.* (2000) Minor lesion mutational spectrum of the entire *NF1* gene does not explain its high mutability but points to a functional domain upstream of the GAP-related domain. Am J Hum Genet 66: 790–818.

Frommolt P, Abdallah AT, Altmüller J, *et al.* (2012) Assessing the enrichment performance in targeted resequencing experiments. Hum Mutat 33:635–641.

Gasparini P, D'Agruma L, Pio de Cillis G, *et al.* (1996) Scanning the first part of the neurofibromatosis type 1 gene by RNA-SSCP: identification of three novel mutations and of two new polymorphisms. Hum Genet 97:492–495.

Han SS, Cooper DN, Upadhyaya MN (2001) Evaluation of denaturing high performance liquid chromatography (DHPLC) for the mutational analysis of the neurofibromatosis type 1 (NF1) gene. Hum Genet 109:487–497.

Hattori M, Torii C, Yagihashi T, *et al.* (2009) Diagnosis of Russell-Silver syndrome by the combined bisulfite restriction analysis—denaturing high-performance liquid chromatography assay. Genet Test Mol Biomarkers 13:623–630.

Japanese Genetic Variation Consortium (2013) Human genetic variation browser. Available at www.genome.med.kyoto-u.ac.jp/SnpDB (accessed March 18 2014).

Jones K (2005) Smith's Recognizable Patterns of Human Malformation. Saunders, Philadelphia.

Kosaki K, Udaka T, Okuyama T (2005) DHPLC in clinical molecular diagnostic services. Mol Genet Metab 86:117–123.

Kumar P, Henikoff S, Ng PC (2009) Predicting the effects of coding non-synonymous variants on protein function using the SIFT algorithm. Nat Protoc 4:1073–1081.

Lee MJ, Su YN, You HL, *et al.* (2006) Identification of forty-five novel and twenty-three known *NF1* mutations in Chinese patients with neurofibromatosis type 1. Hum Mutat 27:832.

Li H, Durbin R (2009) Fast and accurate short read alignment with Burrows-Wheeler Transform. Bioinformatics 25:1754–1760.

Li Y, Bollag G, Clark R, *et al.* (1992) Somatic mutations in the neurofibromatosis 1 gene in human tumors. Cell 69:275–281.

McKenna A, Hanna M, Banks E, *et al.* (2010) The Genome Analysis Toolkit: a MapReduce framework for analyzing next-generation DNA sequencing data. Genome Res 20: 1297–1303.

Messiaen LM, Callens T, Mortier G, *et al.* (2000) Exhaustive mutation analysis of the *NF1* gene allows identification of 95% of mutations and reveals a high frequency of unusual splicing defects. Hum Mutat 15:541–555.

Nemethova M, Bolcekova A, Ilencikova D, *et al.* (2013) Thirty-nine novel neurofibromatosis 1 (NF1) gene mutations identified in Slovak patients. Ann Hum Genet 77:364–379.

Neurofibromatosis Conference Statement (1988) National Institutes of Health Consensus Development Conference. Arch Neurol 45:575–578.

Purandare SM, Huntsman Breidenbach H, *et al.* (1995) Identification of neurofibromatosis 1 (NF1) homologous loci by direct sequencing, fluorescence *in situ* hybridization, and PCR amplification of somatic cell hybrids. Genomics 30:476–485.

Purandare SM, Lanyon WG, Connor JM (1994) Characterisation of inherited and sporadic mutations in neurofibromatosis type-1. Hum Mol Genet 3:1109–1115.

Richards CS, Bale S, Bellissimo DB, *et al.* (2008) ACMG recommendations for standards for interpretation and reporting of sequence variations: revisions 2007. Genet Med 10: 294–300.

Rozen S, Skaletsky H (2000) Primer3 on the www for general users and for biologist programmers. Methods Mol Biol 132:365–386.

Sabbagh A, Pasmant E, Imbard A, *et al.* (2013) NF1 molecular characterization and neurofibromatosis type I genotype-phenotype correlation: the French experience. Hum Mutat 34: 1510–1518.

Samejima H, Torii C, Kosaki R, *et al.* (2007) Screening for Alagille syndrome mutations in the *JAG1* and *NOTCH2* genes using denaturing high-performance liquid chromatography. Genet Test Mol Biomarkers 11:216–227.

Schwarz JM, Rödelsperger C, Schuelke M, *et al.* (2010) MutationTaster evaluates disease-causing potential of sequence alterations. Nat Methods 7:575–576.

Siepel A, Pollard KS, Haussler D (2009) New methods for detecting lineage-specific selection. Proceedings of the 10th International Conference on Research in Computational. Mol Biol 3909:190–205.

Takenouchi T, Hida M, Sakamoto Y, *et al.* (2013a) Severe congenital lipodystrophy and a progeroid appearance: mutation in the penultimate exon of *FBN1* causing a recognizable phenotype. Am J Med Genet A 161A:3057–3062.

Takenouchi T, Matsuzaki Y, Torii C, *et al.* (2014) *SOX9* dimerization domain mutation mimicking type 2 collagen disorder phenotype. Eur J Med Genet 57:298–301.

Takenouchi T, Shimizu A, Torii C, *et al.* (2013b) Multiple Café au Lait spots in familial patients with *MAP2K2* mutation. Am J Med Genet A 164A:392–396.

Teer JK, Green ED, Mullikin JC, *et al.* (2012) VarSifter: visualizing and analyzing exome-scale sequence variation data on a desktop computer. Bioinformatics 28:599–600.

Thorvaldsdóttir H, Robinson JT, Mesirov JP (2013) Integrative Genomics Viewer (IGV): high-performance genomics data visualization and exploration. Brief Bioinform 14:178–192.

Udaka T, Imoto I, Aizu Y, *et al.* (2007) Multiplex PCR/liquid chromatography assay for screening of subtelomeric rearrangements. Genet Test Mol Biomarkers 11:241–248.

Udaka T, Kurosawa K, Izumi K, *et al.* (2006) Screening for partial deletions in the *CREBBP* gene in Rubinstein-Taybi syndrome patients using multiplex PCR/liquid chromatography. Genet Test Mol Biomarkers 10:265–271.

Udaka T, Torii C, Takahashi D, *et al.* (2005) Comprehensive screening of the thiopurine methyltransferase polymorphisms by denaturing high-performance liquid chromatography. Genet Test Mol Biomarkers 9:85–92.

Upaddhyaya M (2008) *NF1* gene structure and *NF1* genotype/phenotype correlations. In: Kaufmann D (ed) Neurofibromatoses. Karger, Basel, pp 46–62.
Valero MC, Martín Y, Hernández-Imaz E, *et al.* (2011) A highly sensitive genetic protocol to detect NF1 mutations. J Mol Diagn 13:113–122.
Yan D, Tekin M, Blanton SH, *et al.* (2013) Next-generation sequencing in genetic hearing loss. Genet Test Mol Biomarkers 17:581–587.

Address correspondence to:
Kenjiro Kosaki, MD, FACMG
Center for Medical Genetics
Keio University School of Medicine
35 Shinanomachi, Shinjuku-ku
Tokyo 160-8582
Japan

E-mail: kkosaki@z3.keio.jp

nature COMMUNICATIONS

ARTICLE

Received 8 Dec 2013 | Accepted 31 Jan 2014 | Published 26 Feb 2014

DOI: 10.1038/ncomms4368

Regulation of MKL1 via actin cytoskeleton dynamics drives adipocyte differentiation

Hiroyuki Nobusue[1,2], Nobuyuki Onishi[2], Takatsune Shimizu[2,3], Eiji Sugihara[2,3], Yoshinao Oki[1], Yuko Sumikawa[1], Tatsuyuki Chiyoda[2], Koichi Akashi[4], Hideyuki Saya[2,3] & Koichiro Kano[1]

Cellular differentiation is regulated through activation and repression of defined transcription factors. A hallmark of differentiation is a pronounced change in cell shape, which is determined by dynamics of the actin cytoskeleton. Here we show that regulation of the transcriptional coactivator MKL1 (megakaryoblastic leukemia 1) by actin cytoskeleton dynamics drives adipocyte differentiation mediated by peroxisome proliferator-activated receptor γ (PPARγ), a master transcriptional regulator of adipogenesis. Induction of adipocyte differentiation results in disruption of actin stress fibres through downregulation of RhoA-ROCK signalling. The consequent rapid increase in monomeric G-actin leads to the interaction of G-actin with MKL1, which prevents nuclear translocation of MKL1 and allows expression of PPARγ followed by adipogenic differentiation. Moreover, we found that MKL1 and PPARγ act in a mutually antagonistic manner in the adipocytic differentiation programme. Our findings thus provide new mechanistic insight into the relation between the dynamics of cell shape and transcriptional regulation during cellular differentiation.

[1] Laboratory of Cell and Tissue Biology, College of Bioresource Sciences, Nihon University, Fujisawa, Kanagawa 252-0880, Japan. [2] Division of Gene Regulation, Institute for Advanced Medical Research, Keio University School of Medicine, Tokyo 160-8582, Japan. [3] Japan Science and Technology Agency, Core Research for Evolutional Science and Technology (CREST), Tokyo 102-0076, Japan. [4] Department of Medicine and Biosystemic Science, Kyushu University Graduate School of Medical Science, Fukuoka 812-8582, Japan. Correspondence and requests for materials should be addressed to H.S. (email: hsaya@a5.keio.jp) or to K.K. (email: kano.kouichirou@nihon-u.ac.jp).

Activation and repression of defined transcription factors are essential for the commitment of progenitors to a specific differentiation lineage, setting the stage for a gene expression pattern characteristic of each mature cell type[1–3]. Adipocyte differentiation is regulated by multiple transcription factors, with PPARγ and members of the CCAAT/enhancer-binding protein (C/EBP) family having central roles. Cooperative interactions among these transcription factors drive the expression of downstream target genes that are necessary for the generation and maintenance of adipocyte characteristics such as lipid accumulation and insulin sensitivity[4]. The key role of PPARγ in the commitment of mesenchymal precursors to the adipocytic differentiation programme is evident from the observation that forced expression of this protein stimulates adipogenesis in nonadipogenic fibroblastic cell lines, such as NIH 3T3 and 3T3-C2 (refs 5,6). PPARγ is thus thought to function as an adipocyte-specific master switch in acquisition of the adipocytic phenotype[7].

The adipocytic differentiation of fibroblastic preadipocytes is accompanied by the adoption of a rounded morphology that is characteristic of mature adipocytes and allows for maximal lipid storage[8]. Cell morphology is determined primarily by the actin cytoskeleton[9]. Adipocyte differentiation is thus associated with a shift in the structures formed by filamentous (F) actin from stress fibres to cortical fibres[10,11]. The relation between such reorganization of the actin cytoskeleton and the PPARγ-mediated adipocytic differentiation programme has remained unclear, however.

We have previously established a preadipocyte cell line derived from mouse dedifferentiated fat (DFAT) cells and which possesses a higher potential to differentiate into adipocytes compared with the mouse preadipocyte cell line 3T3-L1 (ref. 12). Unlike 3T3-L1 cells, these DFAT cells do not undergo spontaneous adipogenesis, with the adipocytic differentiation of DFAT cells thus being more tightly controlled than that of 3T3-L1 cells[12,13]. Here, we examine the roles of actin cytoskeleton remodelling in adipocytic differentiation by using DFAT cells. We show that the rapid disruption of actin stress fibres through downregulation of RhoA-ROCK signalling and the consequent increase in monomeric G-actin levels are observed before adipocyte differentiation. We also found that interaction of monomeric G-actin with the transcriptional coactivator MKL1 is the key event for initiating PPARγ expression. Moreover, MKL1 and PPARγ were shown to act in a mutually antagonistic manner in the adipocytic differentiation programme. Our findings provide a new insight into the regulatory mechanism of adipocyte differentiation.

Results

Adipogenesis requires disruption of actin stress fibres. We first examined the changes in the actin cytoskeleton and PPARγ expression during adipogenesis with the use of an established DFAT cell line. Before induction of adipogenesis, DFAT cells manifest a fibroblastic morphology with well-developed actin stress fibres (Fig. 1a). At 24 h after the induction of adipocytic differentiation with the combination of 3-isobutyl-1-methylxanthine (IBMX), dexamethasone and insulin, the cells exhibit a well-spread morphology associated with the disruption of most stress fibres (Fig. 1a,c; Supplementary Movie 1). The upregulation of PPARγ expression at both mRNA and protein levels is evident at 48 h (Fig. 1a,b), at which time the cell morphology has become stellate and the cortical actin structures characteristic of adipocytes are evident (Fig. 1a). The expression of perilipin (a marker of terminal adipocyte differentiation) and the accumulation of lipid droplets are observed from 60 h, at which time the cell morphology has become more rounded (Fig. 1a). Together, these results thus suggested that disruption of actin stress fibres precedes the induction of PPARγ expression during adipocyte differentiation.

Previous studies have shown that actin cytoskeleton dynamics associated with cell rounding in response to mechanical or physical stimuli (such as matrix stiffness and cytoskeletal tension) result in adipogenic differentiation of 3T3-F442A preadipocytes or mesenchymal stem cells by a mechanism that involves RhoA-ROCK (Rho-kinase) signalling[14–18], which regulates the formation of actin stress fibres and focal adhesions[19,20]. On the other hand, ectopic expression of PPARγ in mesenchymal stem cells or NIH 3T3 fibroblasts has been found to induce not only expression of adipose-specific genes but also morphological differentiation, including the accumulation of triglyceride droplets[5,21–24]. It has remained unknown, however, whether the pathways underlying the induction of adipogenesis either by PPARγ or by changes in cell shape operate independently of each other or in an interdependent manner. To address this question, we tested the effects both of RNA interference (RNAi)-mediated depletion of cofilin1, a protein that promotes the disassembly of actin filaments[25], and of phalloidin (a cytoskeletal fixative) on PPARγ expression during adipocyte differentiation. Either knockdown of cofilin1 with specific small interfering RNAs (siRNAs) or treatment with phalloidin blocked the disruption of actin stress fibres as well as markedly inhibited both the upregulation of PPARγ and PPARγ target gene expression and the accumulation of lipid droplets elicited by inducers of adipocyte differentiation in DFAT cells and 3T3-L1 preadipocytes (Fig. 1d,e; Supplementary Fig. 1). These data thus indicated that the disruption of actin stress fibres is required

Figure 1 | Disruption of actin stress fibres is required for adipocyte differentiation. (**a**) Fluorescence microscopy of the actin cytoskeleton (stained with phalloidin) as well as of PPARγ or perilipin expression during adipogenesis in DFAT cells. Nuclei were stained with Hoechst 33342 (blue fluorescence). Scale bars, 20 μm. (**b**) Relative abundance of *Pparg* mRNA during adipocytic differentiation in DFAT cells (left panel). (**a–f**) $P<0.05$, Tukey's honest significant difference test. A nuclear fraction prepared from the cells was also subjected to immunoblot analysis of PPARγ and lamin C (loading control) (right panel). (**c**) Time-lapse imaging of DFAT cells expressing red fluorescent protein (RFP)-tagged actin at the indicated times (hours:minutes). Scale bars, 50 μm. (**d**) 3T3-L1 preadipocytes transfected with cofilin1 (si*Cfl1*-a) or control (si*Control*) siRNAs were exposed to inducers of differentiation for 96 h. They were then subjected to fluorescence microscopic analysis of the actin cytoskeleton and PPARγ expression. Nuclei were stained with Hoechst 33342. Scale bars, 50 μm. Relative abundance of *Pparg*, *Cebpa*, *Fabp4*, *Slc2a4* and *Plin1* mRNAs. *$P<0.05$, Student's *t*-test. (**e**) Oil red O (ORO) staining of cells treated as in **d**. Bars, 100 μm. The absorbance at 510 nm (A_{510}) of dye extracted from the stained cells was also determined. *$P<0.05$, Student's *t*-test. (**f**) Immunoblot analysis of active and total forms of Rho proteins during adipocyte differentiation in DFAT cells (left panels). GAPDH was examined as a loading control. Quantification of the immunoblotting data was performed using densitometry. Data were normalized to the amount of total Rho (right panel). *$P<0.05$, Student's *t*-test. n.s., not significant. (**g**) Fluorescence microscopy of the actin cytoskeleton as well as of PPARγ or perilipin expression in DFAT cells expressing HA-tagged RhoAV14 or RhoAN19 and exposed for 96 h to inducers of differentiation in the absence or presence of Y-27632 (30 μM) or CytD (0.2 μM). Nuclei were stained with Hoechst 33342. Scale bars, 20 μm. At least 50 HA-positive cells were scored for determination of the percentage of those expressing PPARγ. *$P<0.05$, Student's *t*-test. All quantitative data are means ± s.d. ($n=3$ experiments fibres).

for the induction of PPARγ expression during adipocyte differentiation.

RhoA-ROCK signalling regulates adipogenesis. We next investigated whether RhoA-ROCK signalling plays a role in adipogenic differentiation dependent on the disruption of actin stress fibres in DFAT cells. The GTP-bound (active) form of Rho proteins was detected at a high level before adipogenic induction and was markedly reduced in abundance within 24 h after exposure of the cells to inducers of adipocyte differentiation

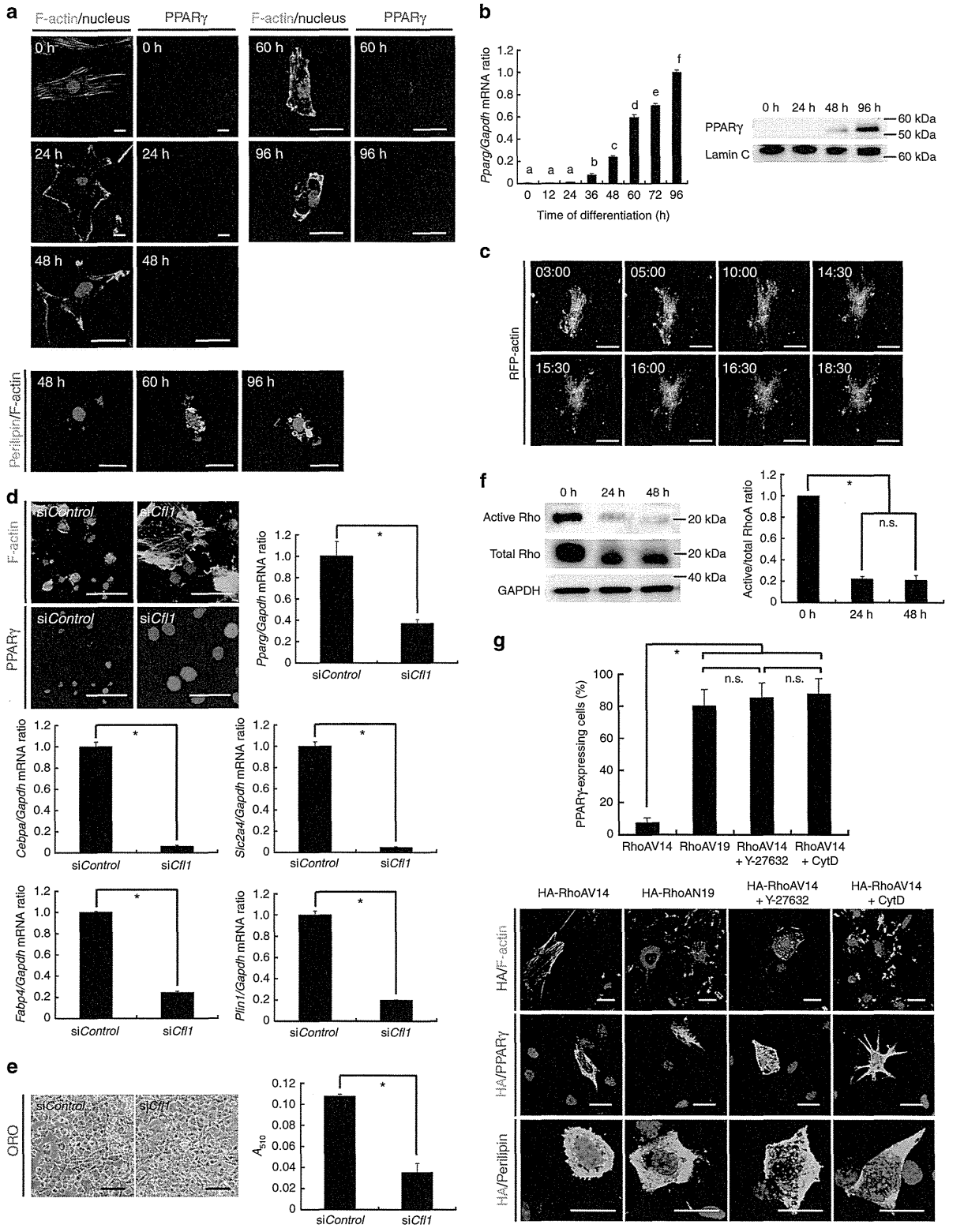

(Fig. 1f). We transiently transfected DFAT cells with plasmids encoding hemagglutinin epitope (HA)–tagged dominant active (RhoAV14) or dominant negative (RhoAN19) mutants of RhoA and then exposed the cells to inducers of adipocytic differentiation for 96 h. Expression of RhoAV14 inhibited both remodelling of the actin cytoskeleton as well as the induction of PPARγ and perilipin expression, and these inhibitory effects were prevented by treatment with the ROCK inhibitor Y-27632 (Fig. 1g). We also determined whether the effects of ROCK inhibition in RhoAV14-expressing cells were mimicked by the actin-depolymerizing agent cytochalasin D (CytD). The addition of CytD indeed restored remodelling of the actin cytoskeleton as well as the expression of PPARγ and perilipin in RhoAV14-expressing cells to levels similar to those apparent in RhoAV14-expressing cells treated with Y-27632 or in cells expressing RhoAN19 (Fig. 1g). These results thus indicated that RhoA-ROCK signalling regulates adipocyte differentiation through control of remodelling of the actin cytoskeleton.

G-actin induces adipogenesis by controling MKL1 localization. Recent studies have identified mechanisms by which actin dynamics directly affect gene transcription[26]. Monomeric G-actin binds to the transcriptional coactivator MKL1 (also known as MAL or MRTF-A) and prevents it from translocating to the nucleus and activating transcription[27,28]. Furthermore, in multipotent mesenchymal stem cells, Med23 functions as a molecular switch between ELK1 and MKL1 that controls differentiation into adipocytes or smooth muscle cells[29], suggesting links between MKL1 and adipogenesis. To explore whether the control of MKL1 translocation by cellular G-actin contributes to the regulation of PPARγ expression and adipocyte differentiation, we established DFAT cells expressing mCherry fused to MKL1 (mCherry-MKL1; Supplementary Fig. 2a) and investigated G-actin levels and mCherry-MKL1 localization before and after the induction of adipocyte differentiation. F-actin was rapidly depolymerized to monomeric G-actin after the induction of adipocyte differentiation, with the increase in cellular G-actin concentration (Fig. 2a). mCherry-MKL1 was detected exclusively in the nucleus before adipogenic induction but was predominantly pancellular and/or cytoplasmic after the induction of adipogenesis (Fig. 2a). PPARγ expression was detected in cells having the cytoplasmic localization of mCherry-MKL1 (Supplementary Fig. 2b).

We next tested whether actin-depolymerizing agents latrunculin A (LatA), which increases monomeric G-actin[27,30], or swinholide A (SwinA), which increases dimeric actin that does not interact with MKL1 (refs 27,30,31), might mimic the effects of inducers of adipogenesis on dynamics of the actin cytoskeleton and MKL1 localization in DFAT cells expressing mCherry-MKL1. Indeed, LatA or SwinA induced disruption of actin stress fibres and increased the cellular abundance of G-actin monomers or dimers, respectively (Fig. 2b; Supplementary Fig. 2c). LatA treatment caused the cytoplasmic sequestration of mCherry-MKL1, whereas SwinA treatment resulted in the nuclear localization (Fig. 2b). Furthermore, LatA alone induced a significant increase in the expression of PPARγ and PPARγ target genes unlike SwinA (Fig. 2c,d). These results suggested that monomeric G-actin formation leads to adipocyte differentiation by blocking the nuclear import of MKL1, but not by other consequences of disruption of actin stress fibres. Similarly to LatA, treatment with Y-27632, elicited disruption of actin stress fibres and the cytoplasmic sequestration of MKL1, resulting in a marked increase in the expression of PPARγ and PPARγ-target genes as well as in the accumulation of lipid droplets in DFAT cells and 3T3-L1 preadipocytes (Supplementary Fig. 3).

Adipogenesis requires interaction between G-actin and MKL1. We also asked whether the interaction between G-actin and MKL1 and the consequent cytoplasmic sequestration of MKL1 contribute to adipocyte differentiation. To address this issue, we established DFAT cells and 3T3-L1 preadipocytes that express a FLAG epitope–tagged fusion protein of the oestrogen receptor (ER) and either MKL1 or a deletion mutant of MKL1 (MKL1-N100) that lacks the 100 NH_2-terminal amino acids of the full-length protein and therefore does not contain the RPEL actin-binding domain[32,33] (Supplementary Fig. 4a). Exposure of these cells to the ER agonist 4-hydroxytamoxifen (TAM) induced the nuclear translocation of each fusion protein (Fig. 3a). The nuclear translocation of ER-MKL1 was accompanied by a marked decrease in the expression of PPARγ and PPARγ target genes as well as in the accumulation of lipid droplets in cells also exposed to inducers of adipocytic differentiation (Fig. 3b–d; Supplementary Fig. 4b–d). Moreover, expression of ER-MKL1-N100, which fails to bind G-actin and a substantial proportion of which was localized to the nucleus even in the absence of TAM (Fig. 3b; Supplementary Fig. 4b), resulted in marked suppression of adipogenesis in the absence or presence of TAM compared with that apparent in cells expressing ER-MKL1 (Fig. 3b–d; Supplementary Fig. 4b–d). We also tested if ER-MKL1-N100 reverts the effects elicited by treatment with LatA in DFAT cells and 3T3-L1 preadipocytes. The expression of ER-MKL1-N100, which was predominantly localized to the nucleus even after treatment with LatA and remarkably impaired the expression of PPARγ and PPARγ target genes compared with that of ER-MKL1 (Fig. 3e,f; Supplementary Fig. 4e,f). These findings significantly strengthen our conclusion that the increase in the cytoplasmic abundance of G-actin triggers adipocyte differentiation via regulation of the subcellular localization of MKL1.

Loss of MKL1 drives adipocyte differentiation. We further assessed whether RNAi-mediated depletion of MKL1 alone might induce PPARγ expression and adipocyte differentiation in the absence of an adipogenic cocktail. In both DFAT cells and 3T3-L1

Figure 2 | The increase of G-actin accumulation resulting from disruption of actin stress fibres is involved in the cytoplasmic sequestration of MKL1 and adipocyte differentiation in DFAT cells. (**a**) Immunofluorescence analysis of mCherry and G-actin (stained with DNase I) in cells stably expressing mCherry-MKL1 at 0 or 48 h after the induction of adipogenesis(upper panels). Nuclei were stained with Hoechst 33342. Scale bars, 100 μm. At least 300 cells per coverslip were scored for determination of the percentage of the subcellular localization of MKL1 (lower panel). N, nuclear; N/C, comparable intensity in nucleus and cytoplasm; C, cytoplasmic. (**b**) Immunofluorescence analysis of mCherry and G-actin in mCherry-MKL1-expressing cells exposed to Lat A (0.4 μM), Swin A (0.1 μM) or dimethyl sulfoxide (DMSO, control) for 6 h in growth medium without an adipogenic cocktail (upper panels). Nuclei were stained with Hoechst 33342. Scale bars, 50 μm. Quantitation of immunofluorescence microscopy; localization of the indicated mCherry-MKL1 was scored in 300 cells as in panel **a** (lower panel). (**c**) Relative abundance of *Pparg*, *Cebpa*, *Fabp4*, *Slc2a4*, and *Plin1* mRNAs in cells treated as in **b**. ND, not detected. (**d**) Cells treated as in **b** were cultured for an additional 18 h (total of 24 h) and then subjected to immunofluorescence analysis of mCherry and PPARγ expression. Nuclei were stained with Hoechst 33342. Scale bars, 50 μm. All quantitative data are means ± s.d. ($n = 3$ experiments). *$P < 0.05$, Student's *t*-test.

preadipocytes, knockdown of *Mkl1* expression (Supplementary Fig. 5a) resulted in a marked increase both in the expression of PPARγ and PPARγ target genes as well as in the extent of lipid droplet accumulation (Fig. 4a; Supplementary Fig. 5b,c). Moreover, we found that depletion of MKL1 alone resulted in a marked increase in the expression of PPARγ and PPARγ target genes even in NIH 3T3 nonadipogenic fibroblasts (Fig. 4b; Supplementary Fig. 5a). These findings indicated that loss of MKL1 function elicits PPARγ expression and adipocyte differentiation *in vitro*.

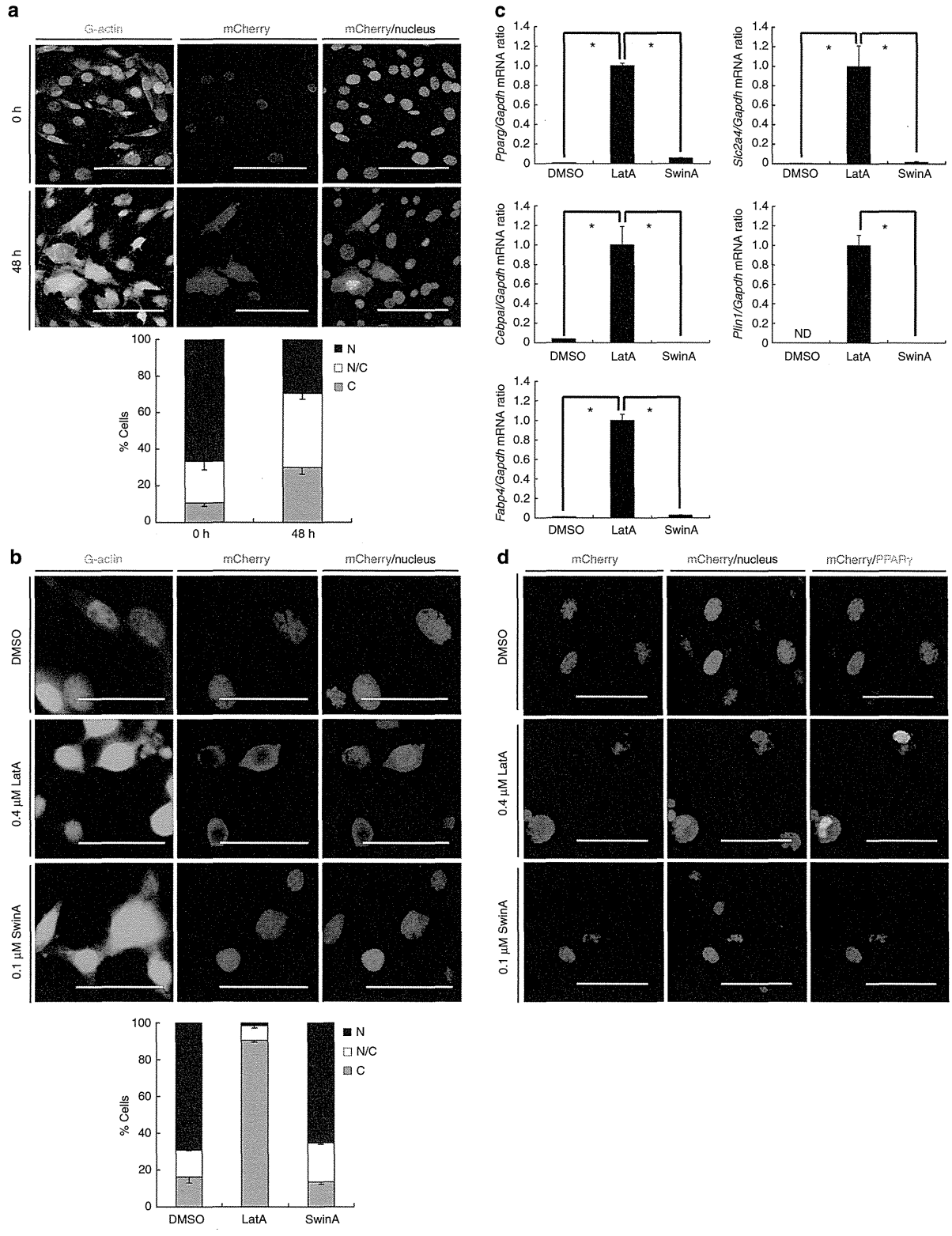

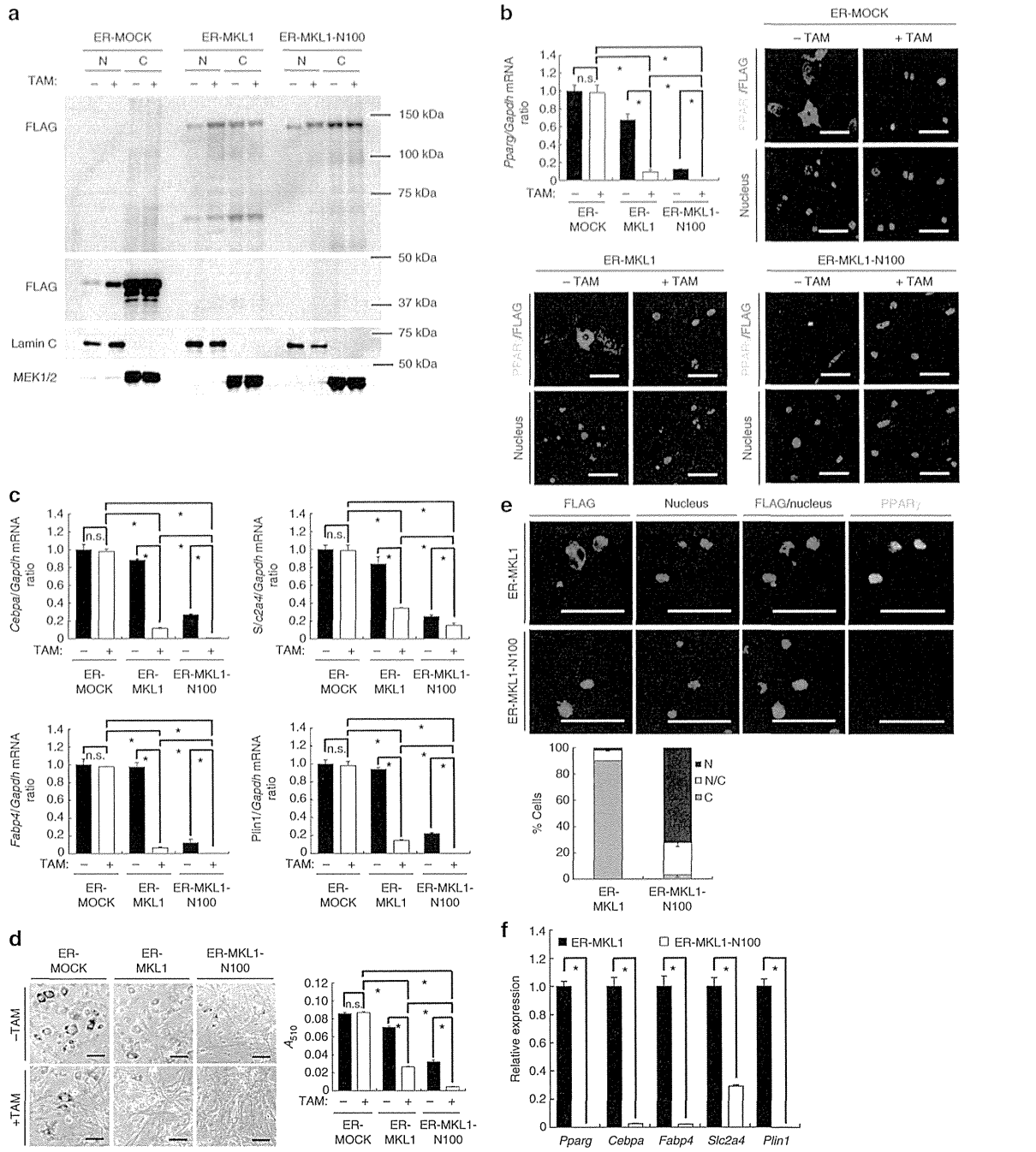

Figure 3 | Interaction between G-actin and MKL1 and the consequent cytoplasmic sequestration of MKL1 are required for adipocytic differentiation in DFAT cells. (**a**) Cells stably expressing 3 × FLAG-tagged ER (ER-MOCK, control), ER-MKL1 or ER-MKL1-N100 were exposed for 48 h to inducers of adipogenic differentiation in the absence or presence of TAM (1 μM), after which nuclear (N) and cytoplasmic (C) fractions were prepared from the cells and subjected to immunoblot analysis of FLAG, lamin C (nuclear marker) and MEK1/2 (cytoplasmic marker). (**b**) Cells treated as in **a** were analysed for the relative abundance of *Pparg* mRNA or subjected to immunofluorescence analysis of FLAG and PPARγ. Nuclei were stained with Hoechst 33342. Scale bars, 50 μm. (**c**) Relative abundance of *Cebpa*, *Fabp4*, *Slc2a4* and *Plin1* mRNAs in cells treated as in **a**. (**d**) Cells treated as in **a** were cultured for an additional 48 h (total of 96 h) and then stained with oil red O. Scale bars, 100 μm. The A_{510} of dye extracted from the stained cells was also determined. n.s., not significant. (**e**) Cells stably expressing ER-MKL1 or ER-MKL1-N100 were exposed for 24 h to Lat A (0.4 μM) in the presence of TAM (1 μM) and then subjected to immunofluorescence analysis of FLAG and PPARγ (upper panels). Nuclei were stained with Hoechst 33342. Scale bars, 50 μm. At least 300 cells per coverslip were scored for determination of the percentage of the subcellular localization of MKL1 (centre panel). N, nuclear; N/C, comparable intensity in nucleus and cytoplasm; C, cytoplasmic. (**f**) Relative abundance of *Pparg*, *Cebpa*, *Fabp4*, *Slc2a4* and *Plin1* mRNAs in cells treated as in **e**. All quantitative data are means ± s.d. ($n = 3$ experiments). *$P < 0.05$, Student's *t*-test.